Along the Channel Gradients Impact on the Spatioactivity of Gas Diffusion Electrodes at High Conversions during CO_2 Electroreduction

Kas, Recep; Star, Andrew G.; Yang, Kailun; Van Cleve, Tim; Neyerlin, Kenneth C.; Smith, Wilson A.

DOI
10.1021/acssuschemeng.0c07694

Publication date
2021

Document Version
Accepted author manuscript

Published in
ACS Sustainable Chemistry and Engineering

Along the Channel Gradients Impact on the Spatioactivity of Gas Diffusion Electrodes at High Conversions during CO_2 Electroreduction

Recep Kas[a,b*], *Andrew G. Star*[a], *Kailun Yang*[d], *Tim Van Cleve*[a], *K.C. Neyerlin*[a], *Wilson A. Smith*[a,b,c,d],

[a]National Renewable Energy Laboratory, Golden, Colorado 80401, United States

[b] Renewable and Sustainable Energy Institute (RASEI), University of Colorado Boulder, Boulder, CO 80303, USA

[c] Department of Chemical and Biological Engineering, University of Colorado Boulder, Boulder, CO 80303, USA

[d] Materials for Energy Conversion and Storage (MECS), Department of Chemical Engineering, Faculty of Applied Sciences, Delft University of Technology, van der Maasweg 9, 2629 HZ Delft, The Netherlands

Corresponding Authors*: recep.kas@colorado.edu, wilson.smith@colorado.edu

KEYWORDS: Electrochemical CO_2 reduction, Modelling study, Single pass conversion, Concentration overpotential, Local pH

ABSTRACT

Results of a 2-D transport model for a gas diffusion electrode performing CO_2 reduction to CO with a flowing catholyte are presented, including the concentration gradients along the flow cell, spatial distribution of the current density and local pH in the catalyst layer. The model predicts that both the concentration of CO_2 and the buffer electrolyte gradually diminish along the channels for a parallel flow of gas and electrolyte as a result of electrochemical conversion and non-electrochemical consumption. At high single-pass conversions, significant concentration gradients exist along the flow channels leading to large local variations in the current density (>150 mA/cm^2), which becomes prominent when compared to ohmic losses. In addition, concentration overpotentials change dramatically with CO_2 flow rate, which results in significant differences in outlet concentrations at high conversions. The outlet concentration of CO attains a maximum of 80% along with 5 % CO_2 and 15% H_2, although the maximum single-pass conversion is limited to below 60% due to homogenous consumption by the electrolyte. Fundamental and practical implications of our findings on electrochemical CO_2 reduction are discussed with a focus on the tradeoff between high current density operation and high single-pass conversion efficiency.

INTRODUCTION

Electrochemical CO_2 reduction has received increased interest from researchers during the last decade, primarily motivated to close the carbon cycle and store electricity in energy dense chemicals and fuels[1, 2]. While a majority of the work has been devoted to catalyst development in CO_2 saturated aqueous solutions, recently a noticeable shift to vapor-fed and flowing systems has been used to reach production rates closer to economic feasibility.[3-8] Although the energy efficiency, activity and stability of CO_2 reduction catalysts and systems are still not in the desired range for commercialization, the shift to vapor-fed systems is of high importance to integrate catalyst development and reactor design.[4, 9, 10]

Microfluidic and polymer electrolyte membrane (PEM) reactor designs with different configurations were used for studying electrochemical CO_2 reduction at room temperature, each having particular advantages.[11] Microfluidic flow cells can be operated by using a thin flowing liquid electrolyte between the anode and cathode without a membrane.[12, 13] On the other hand, PEM based flow cells can be operated in a zero-gap configuration by utilizing solid electrolytes

and membranes, however, a flowing liquid electrolyte between membrane and cathode GDE was also commonly used.[11] PEM based reactors with zero-gap configuration containing a membrane electrode assembly (MEA) might offer several advantages over other device architectures that contain a flowing electrolyte such as having lower ohmic drops at high current density, higher volumetric energy density, making them more suitable to scale-up.[14, 15] However, PEM based and microfluidic reactors with flowing liquid catholytes are the most numerous configuration in electrochemical CO_2 reduction so far.[16, 17] Although both flowing electrolyte and gas phase CO_2 might require a delicate pressure balance and more technical control at larger scale and these configurations might suffer from huge ohmic loses at high current density,[14], it has several advantages especially for cathodes that are producing liquid products. Electrochemical studies and half cell catalyst screening is less complicated when the catalyst layer(CL) and membrane is separated by liquid catholyte.[15] The flowing electrolyte assures enough water supply for the electrochemical CO_2 reduction as well as refreshes the catholyte that is prone to carbonation and salt precipitation. Overall, these advantages provide a more convenient platform to study half-cell cathodic reactions to investigate and monitor catalytic properties and effects of process conditions. The studies in gas-fed electrochemical cells with flowing liquid catholyte provided crucial information on the effect of process conditions and material parameters to the selectivity and activity of the electrocatalytic process.[14] In addition, a liquid electrolyte layer may be beneficial for cathodes producing non-volatile liquid products such as formic acid and ethanol unlike zero-gap MEA configurations which might suffer from mass transport losses associated with flooding.[18, 19] An alternative promising approach to produce concentrated formic acid has been introduced by using a zero-gap configuration with a solid-state electrolyte junction, but production of liquid compounds with high pKa values remain a challenge.[20, 21] From both a fundamental and

applied perspective it is important understand the effect of mass transport and process conditions on the performance and catalyst screening in systems with flowing catholyte.

Modelling can provide guidelines for optimal operating conditions and crucial insights on key parameters and factors limiting the performance of electrolyzers. Although optimization of gas diffusion electrodes for CO_2 reduction has been guided primarily by experiments, considerable efforts on modelling have also helped push the technology and performance forward. 1-D models are commonly employed to calculate concentrations of reactants and pH near the gas diffusion electrodes in both neutral and alkaline electrolytes.[4, 22-24] These calculations are not only used to correct the potential on the electrode surface but also to understand electrocatalytic selectivity under different process conditions.[25] Weng et al. reported a comprehensive modelling study of gas diffusion electrodes in a PEM type of reactor with a flowing electrolyte and MEA configurations.[26, 27] Although these 1-D models provide great insights on the effect of process parameters and configurations to the performance of the electrolyzer, they cannot effectively account for the concentration gradients existing along the flow channel at high single-pass conversions. The models are confined to catalyst layer of the GDE having similar limitations at high conversions in which the concentration gradients outside the CL can be prominent.

In this study, we shed light on the concentration gradients in the gas and electrolyte flow channel by a 2-D model which can provide longitudinal information along the flow cell. In doing so, we quantify the extent of concentration overpotentials and ohmic drops throughout the CL across a range of potentials. Various process parameters are modified to explore the effects on the CO_2 mass transfer-limited current density, conversion, and outlet concentrations of CO_2, CO and H_2. Our model suggests that ohmic losses largely determine the current density distributions at low conversion rates where small gradients in concentration exist; however, as the concentration

profiles become less uniform (e.g. high conversions) the uneven electrochemical conversion and non-electrochemical consumption of CO_2 leads to non-uniform performance across the electrode. In addition, higher flow rates benefit from higher production rates, i.e. high current density, at the same single-pass conversion, however, the effect of ohmic drops and loss in selectivity becomes more prominent at high conversions. The ability to understand the interplay between process conditions and local environment will help design more efficient electrolyzer systems.

MODEL DESCRIPTION

The cathode compartment of a PEM based CO_2 electrolyzer with a flowing catholyte configuration was modeled at steady state with a 2-D finite element approach. All the mathematical details and parameters used in the model are given in the supporting information. Here, we describe the coupled physical and chemical phenomena, initial and boundary conditions, and provide some of the key equations, material and process parameters necessary to follow the paper. A schematic representation of the model is shown in Figure 1 with liquid (left/blue) and gas (right/yellow) flow

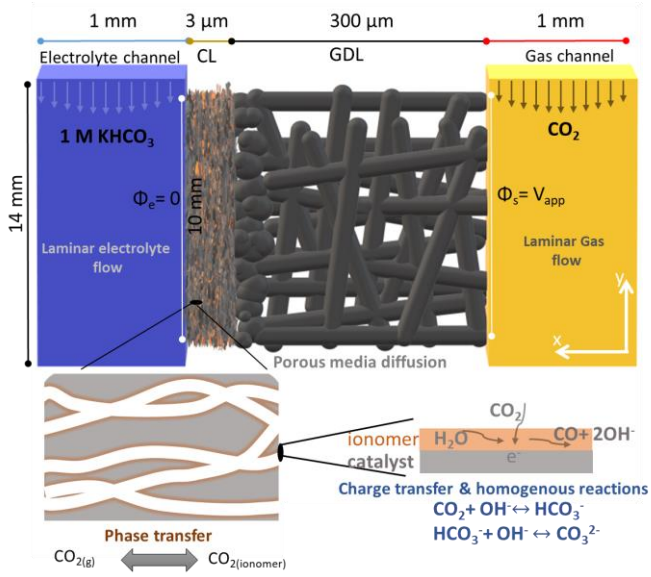

Figure 1: Schematic of the flow cell. Distances are not to scale.

channels in contact with the GDE comprising a gas diffusion layer (GDL) and a catalyst layer (CL). Although the microporous layer was not directly included in the model, the parameters of the GDL were taken from literature that includes a microporous layer.[28] This is a commonly used approach since the key parameters such as permeability, porosity, and conductivity of the GDLs were usually reported as a whole rather than each individual contributions of micro and macroporous layers.[27, 29] The relevant material, dimensional and process parameters used in the simulations are given in Figure 1 and Table 1, with additional parameters in the supporting information.

In these simulations, gaseous CO_2 was fed into the flow cell via a rectangular 1-mm wide and 14-mm long flow channel with a varying flow rate of 5-15 ml min^{-1} while the outlet was assumed to be at atmospheric pressure (Figure 1). The flow channels were kept slightly longer than the GDE, which is 10 mm long, to account for the gradients that extend in the flow channel and the mixing of the reactants and products. Gas phase mass transport in the flow channel was modeled as a single-phase laminar flow which takes into account multi-component diffusion of gases. The gaseous mass transport inside the GDL and CL layer is mostly diffusion driven and pressure driven convection, which are influenced by the porosity, tortuosity, pore size and permeability of the porous medium. Phase transfer of the gaseous CO_2 to the ionomer takes place at the CL and it is driven by the concentration difference between the catalyst surface and ionomer-gas phase interface. At the ionomer and gas interface, CO_2 was assumed to be in equilibrium with the gaseous CO_2 in the CL.[26] The concentration of gases in the ionomer (c_g^I) at a given partial pressure was calculated by,

$$c_g^I = p_g x_i S_g^I \quad \text{(E1)}$$

Where p_g and x_i is the total gas pressure and mole fraction of gas specie i in the CL and S_g^I is the solubility of the gas in the ionomer. The solubility of the gases can be related to the diffusion coefficients (D_g^I)and permeability of the ionomer(ϵ_g^I) via,

$$\epsilon_g^I = D_g^I S_g^I \tag{E2}$$

The transferred CO_2 and water react electrochemically in the electrolyte phase of the CL to produce CO,

$$CO_2 + H_2O + 2\,e^- \longrightarrow CO + 2OH^- \tag{1}$$

while a very small fraction of unreacted dissolved CO_2 escapes to the electrolyte (Figure SI2). The competing hydrogen evolution reaction (HER) can be written as,

$$2H_2O + 2\,e^- \longrightarrow H_2 + 2OH^- \tag{2}$$

Table 1: Some of the key process and material parameters

Parameter	Value	Units	Reference
Gas flow rate	5-15	ml min^{-1}	
Electrolyte flow rate	1	ml min^{-1}	
GDL porosity	0.75		[28]
GDL permeability	3.5 x 10^{-12}	m^{-2}	[28]
CL porosity	0.4		[30]
CL permeability	1.0 x 10^{-15}	m^{-2}	[29]
Active surface area	1.0 x 10^{7}	m^{-1}	[27]
Solubility of the CO_2 in the ionomer	3.97 x 10^{-4}	mol m^{-3} Pa^{-1}	[31]
Solubility of the CO in the ionomer	2.52 x 10^{-4}	mol m^{-3} Pa^{-1}	[32]
Exchange current density, CO formation	3.3 x 10^{-5}	mA cm^{-2}	[33]
Transfer coefficient, CO formation	0.33		[34]
Exchange current density, HER	3.4 x 10^{-7}	mA cm^{-2}	[35]
Transfer coefficient, HER	0.33		[35]
Standard electrode potential, HER	0.0	V vs RHE	[27]
Standard electrode potential, CO formation	-0.11	V vs RHE	[27]
Geometric area	1.0 x 1.0	cm^2	
Flow channel dimensions	0.1 x 1.4	cm^2	

The electrochemical reduction rate of CO_2 to CO at the electrode was calculated by concentration dependent Butler-Volmer kinetics for a silver cathode via,

$$i_{CO} = -i_{CO}^{0} \frac{c_{CO_2}}{c_{CO_2}^{ref}} \alpha_{H_2O} e^{-\frac{\alpha_{CO_2} F}{RT} \eta_{co}} \quad \text{(E3)}$$

where i_{CO} is partial current density of CO, i_{CO}^{0} is exchange current density for CO formation, c_{CO_2} is concentration of CO_2 in the ionomer, α_{H_2O} is the activity of the water and $\alpha_{co}$is the cathodic transfer coeffcient and $n_{CO}\ is$ overpotential. $C_{CO_2}^{ref}$ is the concentration of the CO_2 in the ionomer at a partial pressure of 1 atm. We assumed that the anodic exponential term becomes negligible compared to cathodic term at potentials evaluated in here. The HER rate was calculated via,

$$i_{H_2} = -i_{H_2}^{0} \alpha_{H_2O} e^{-\frac{\alpha_{H_2} F}{RT} \eta_{H_2}} \quad \text{(E4)}$$

where i_{H_2} is partial current density of H_2, $i_{H_2}^{0}$ is exchange current density for H_2 formation , $\alpha_{H_2}$is the cathodic transfer coeffcient and $n_{H_2}$is overpotential for the reaction 2. We assumed that the flowing liquid electrolyte adjacent to the catalyst layer supplies enough water to the ionomer and the ionomer is in a saturated state for the entirety of the simulations.[25] The protons were assumed to be supplied by water molecules for both reactions 1 and 2, since the proton concentration and proton reduction rates are typically very low in neutral and alkaline media. The electric potential (Φ_s) of the electrode is varied between -0.8 V and -2.0 V vs RHE at the GDL-gas flow channel interface while the electrolyte potential (Φ_e) is set to zero as a reference at the CL-electrolyte flow channel interface. The overpotential(n_j) for reactions 1 and 2 are given by the applied potential difference between the electric potential of GDE (ϕ_s) and solution (ϕ_l) via,

$$n_j = (\phi_s - \phi_l) - (E_i^o - 0.059\text{*pH}) \quad \text{(E5)}$$

where (E_i^o) is the standard electrode potential for reaction i. The homogenous reactions and transport of the electrolyte species at the CL and electrolyte channel were modelled by a reaction-diffusion model which considers homogenous reactions of CO_2 with the electrolyte (reaction 3), the buffer actions (reaction 4) and diffusion in porous medium.

$$CO_2 + OH^- \underset{k_1^b}{\overset{k_1^f}{\Longleftrightarrow}} HCO_3^- \tag{3}$$

$$HCO_3^- + OH^- \underset{k_2^b}{\overset{k_2^f}{\Longleftrightarrow}} CO_3^{2-} + H_2O \tag{4}$$

The conversion (X_{CO_2})values reported in this study refers to electrochemical single-pass conversion of CO_2 to CO (reaction 1) which was calculated by the following equation,

$$X_{CO_2} = \frac{R_{Co,out}}{F_m} \times 100 \tag{E5}$$

where $R_{Co,out}$ is the rate of CO production and F_m is the molar flow rate of the CO_2. The consumption of CO_2 refers to the homogenous reaction of CO_2 with OH^- (reaction 3) and it was calculated was calculated by,

$$Consumpiton = \frac{v_{CO2OH}}{F_m} \times 100 \tag{E6}$$

where v_{CO2OH} is net reaction rate of reaction 3.

An aqueous 1 M $KHCO_3$ solution was modeled to flow via a rectangular 1-mm wide and 1.4-cm long flow channel with a flow rate of 1 ml min^{-1} unless otherwise indicated while the outlet was assumed to be at atmospheric pressure. We assumed that the flowing electrolyte ensures the effect of reactant and electrolyte crossover from and towards the anode compartment and that the concentration profiles are negligible.

All the physical and chemical phenomena were solved collectively in the corresponding domain and coupled via source and sink terms to solve the mass, velocity, current density and pressure distributions inside the flow channels and/or GDE by using COMSOL Multiphysics 5.4. The details of the method are given in the supporting information.

RESULTS AND DISCUSSION

Figure 2 presents the mole fraction distribution of gaseous CO_2 at steady state inside the flow channel and GDE for applied potentials of -1.0 to -1.3 V vs RHE, along with the average current density (J_{CO}) and single-pass conversion (X_{CO2}). The corresponding CO mole fractions can be found in the supporting information (Figure SI3). We first discuss the gradients across the flow channel (x-direction) which are highlighted by contour lines and more apparent at high potentials. When the electrolysis starts, CO_2 and H_2O in the ionomer phase are reduced to CO and H_2 at a certain rate on silver surfaces determined by the applied potential and local reactant concentration. In addition, CO_2 homogenously reacts with the cathodically produced hydroxide to form bicarbonate. The electrochemical conversion and non-electrochemical consumption of CO_2 at the CL creates a concentration gradient across the GDE, which is the main thermodynamic driving force for the transport of the gaseous molecules within the porous medium. In addition, a pressure difference created by the homogenous consumption of CO_2 leads to a convective driving force. Therefore, the slope of the contour lines is mostly determined by the effective diffusion coefficient of CO_2 ($D_{CO_2}^{eff}$) and permeability of the porous GDL(κ_{gdl}) and CL(κ_{cl}) which is directly related to the material parameters of the GDE such as porosity, tortuosity and pore size. In the insets of Figure 2, CO_2 gradient in the catalyst layer is shown and magnified for convenience. Since the thickness of the CL (3µm) is significantly smaller than the GDL (300 µm), the gradient across the CL is negligible and contour lines are almost flat. The uniform CO_2 distribution across the CL in

our model is an agreement with 1-D models for an ideally wetted CL.[27] We note that the gradient across the CL can become significant in partially or fully flooded CL's, even for a very thin layers (e.g.100 nm), since the diffusion coefficient drops dramatically transitioning between gas and electrolyte phases.[22, 24, 27]

The CO_2 concentration gradient along the flow cell (y-direction) is larger and more apparent especially at more negative potentials (Figure 2c and 2d). As the CO_2 travels along the channel, the electrochemical reaction and consumption of CO_2 takes place at the CL of the GDE, resulting in a concentration gradient along the GDE and flow channel. With increasing distance from the inlet, the CO_2 concentration in the feed gas declines while the CO concentration increases (Figure SI3). Higher currents lead to a steeper concentration gradients as both electrochemical and non-electrochemical consumption increases. It is important to note that the single-pass conversion is the descriptive parameter for the extent of these gradients rather than the potential and/or current density, since it is possible to minimize the concentration gradients along the flow channel by increasing the flow rate (Figure SI4). Unlike the transport inside the GDL and CL, the transport of

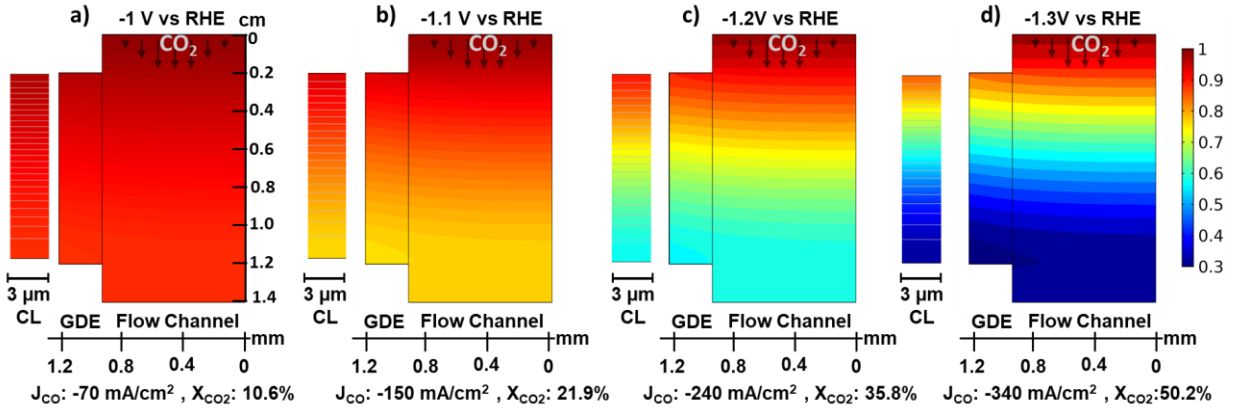

Figure 2: Contour plots of gaseous CO_2 mole fraction in the gas flow channel and GDE for different applied potentials a) -1 V vs RHE b) -1,1 V vs RHE c) -1.2 Vvs RHE d) -1.3 V vs RHE. The corresponding partial current density (J_{CO}) and single-pass conversion (X_{CO2}) are given under each plot. The insets show the gaseous mole fraction of CO_2 in the CL. Flow rate: 5ml min^{-1}. Area of the electrode: 1 cm^2. Both x and y axis correspond to distance and distances are not to scale.

the CO_2 in the flow channel is mostly driven by the forced convective flow from the inlet while the effect of diffusion in the flow channel is relatively small in the y-direction (Peclet number ~ 5). Although the concentration gradients along the flow channel are controlled mostly by convection, the diffusion inside the flow channel even out the concentration gradients along the x-direction. Higher flow rates, i.e. higher Peclet number, might lead to steeper gradients in the x-direction inside the flow channel at the same conversion since there is less time for diffusion to take place. The gradients inside the GDL and CL follow a similar pattern of the flow channel along the flow cell. The concentration gradient along the CL together with the distribution of the (local) pH have a dramatic effect the on performance of the GDE at high conversions. Therefore, it is important to first present pH distributions in the CL before explaining the resultant current distribution, although the former is the result of the latter one.

The two-dimensional distribution of the bicarbonate concentration inside the catalyst and electrolyte flow channel is shown in Figure 3a at an applied potential of -1.0 V vs RHE. During electrochemical CO_2 reduction at the cathode, bicarbonate anions are consumed electrochemically or indirectly by the cathodically produced hydroxide (Equation 3).[36, 37] As a result of the forced

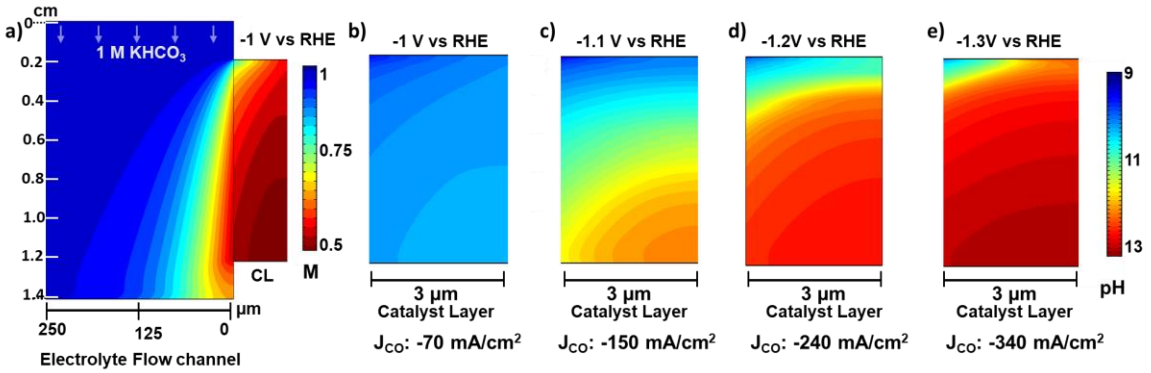

Figure 3: a) Contour plot of bicarbonate concentration in the electrolyte flow channel and CL. **b)** to **e)** The distribution of pH in the CL for different applied potentials. Corresponding average current density is given under each plot. Flow rate: 5ml min^{-1}. Area of the electrode: 1 cm^2. Both x and y axis correspond to distance and distances are not to the scale.

convective flow from the inlet in the y-direction, the decrease in the bicarbonate concentration is apparent along the channel. The boundary thickness for bicarbonate ions increases from a few µm at the inlet to about 200 µm at the outlet as it is consumed along the channel. More negative potentials and/or higher currents result in larger differences in the boundary layer thickness between the outlet and inlet (Figure SI5). Consequently, the buffer capacity along the catalyst layer decreases which has an enormous influence on the distribution of local pH and CO_2 consumption in the catalyst layer.

Figure 3b to 3e present the spatial distribution of local pH in the CL for different applied potentials. The pH near the electrode surface increases at high currents as a result of the production OH^- by CO_2 reduction and water splitting. Although the increase of the pH near the electrode surface is a well-recognized phenomenon on GDEs and solid electrodes,[4, 38-40] the 2-D modelling presented here reveals that the local pH in the CL has a very distinct distribution, since both species (HCO_3^- and CO_2) that can react with $OH^-$are supplied in a parallel flow. The local pH increases almost in a diagonal fashion along the catalyst layer in which the margin between the corners rises as the potential gets more negative. Remarkably, the local pH varies dramatically (>3 pH units) between the inlet and outlet at high potentials. This is a result of spatial distribution of the buffer capacity since the top left and bottom right corners of the catalyst layer have the lowest and highest diffusion layer thickness for bicarbonate ions, respectively. The distribution of the local pH in the catalyst layer also influences the local rate for the non-electrochemical consumption reaction of CO_2 with the hydroxide (Figure SI6). Although, the reaction rate of CO_2 with hydroxide (k_1^f) is orders of magnitude slower (~10^3-10^5) than the bicarbonate (k_2^f), the rate of this reaction significantly rises as the buffer breaks down and there is not enough bicarbonate to react with

hydroxide ions.[38] The CO_2 concentration also diminishes as it travels along the gas flow channel which additionally contributes to the local reaction rate of CO_2 with OH^-. These two joint effects govern the local concentration of the CO_2 in the catalyst layer and thus the local current density.

The current density distributions in the catalyst layer are shown in Figure 4 along with the single-pass conversion values for different applied potentials. The spatial current density distribution exhibits a very similar pattern for all applied potentials, however the current density between the inlet and outlet of the channel changes dramatically along the channel at high potentials as a result of high conversions. In such cases, e.g. -1.3 V vs RHE, there is a current density drop of more than 150 mA/cm^2 between the inlet and outlet. In addition, the current density shows a minimum across the x-direction (a maxima for the contour lines) which becomes less pronounced at higher potentials. Such a current distribution is the result of the combination of the two aforementioned transport effects along the catalyst layer, as well as the ohmic drop across the GDE (Figure SI7). First, decreasing CO_2 concentration along the channel lead to concentration

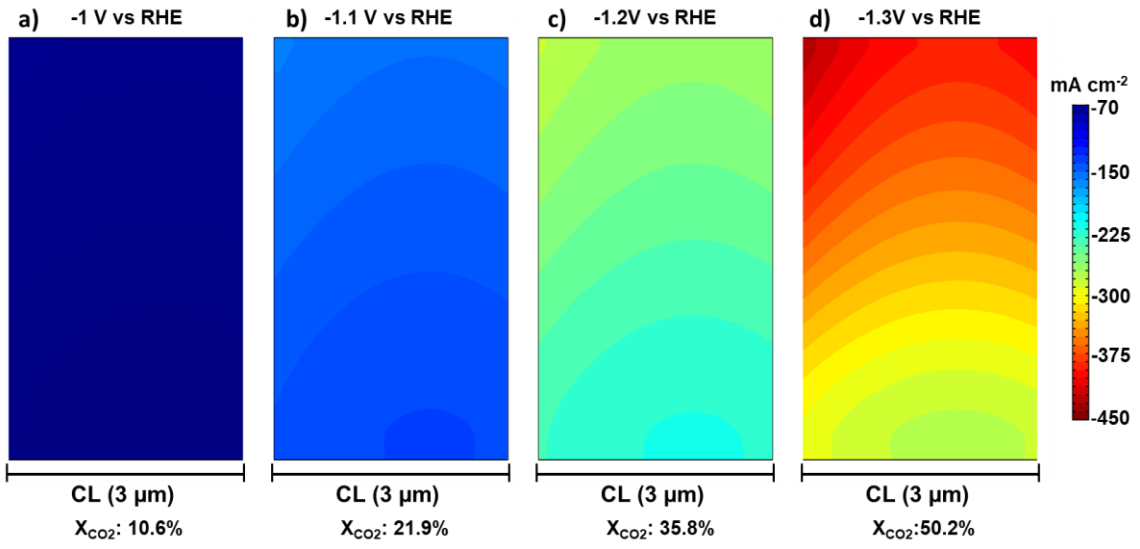

Figure 4: Local partial current density of CO (J_{CO}) in the CL for different applied potentials. The corresponding X_{CO2} is given under each plot. Flow rate: 5ml min^{-1}. Area of the electrode: 1 cm^2.Distances are not to the scale.

overpotentials so that the current density falls from inlet to outlet. Second, the extent of buffer actions also spatially distributed from inlet to outlet which leads to a higher rates homogenous CO_2 consumption at local points with higher alkalinity. Moreover, the applied potential drops across the GDE as a result of the porous structure thus the finite resistance (Figure SI7). The ohmic drops across the CL partially lowers the current density between the inlet and outlet since higher local current densities result in higher ohmic drops. We note that much more complex current distributions might be obtained for fully flooded or partially saturated CLs since the CO_2 concentration varies significantly in the x-direction depending on the saturation level porous medium.[22, 27]

An apparent way of lowering the concentration overpotentials is to increase the gas flow rate at the same applied potential, which comes at the expense of single-pass conversion, for a

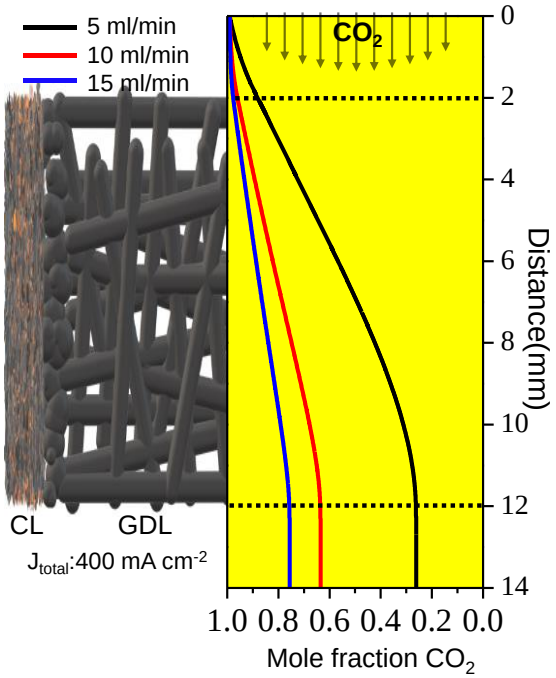

Figure 5*:* Mole fraction of CO_2 in the gas flow channel at a current density of 400 mA cm^{-2} for different flow rates. The dashed lines represent the start and end of the 1 cm long GDE.

given surface area of the electrode (Figure SI4). The effect of the flow rate on the CO_2 mole fraction in the gas channel is given at a current density of 400 mA/cm^2 in Figure 5. The mole fraction of CO_2 drops almost in a linear fashion along the GDE, while the gradients extend towards the inlet of the flow channel for the lowest flow rate. The mole fraction of CO_2 attains a stable value towards the outlet as there is no further production and the reactants and the products are allowed to mix. The extent of the CO_2 gradient along the channel, expectedly, is a strict function of the flow rate of CO_2 gas. Although the extent of the concentration gradients can be considered as significant from this plot, even at the highest flow rate, the effect of concentration gradients on the overall potential losses becomes prominent only at very high single-pass conversions.

The effect of flow rate on the concentration overpotentials and mass transport limited current density is shown in Figure 6a together with and without the ohmic contributions. The difference between the dashed lines and solid lines in Figure 6a represents the potential loses due to the ohmic losses while the difference between the activation-controlled rate (J_{ac}) and the dashed lines represents the concentration overpotentials. Both the current density and the potential within the CL are averaged in this figure and the ohmic resistance here in refers to a combination of the electronic and ionic resistance of the porous GDL and CL. Note that the imaginary reference electrode is placed just at the interface of the CL and electrolyte so there are no ohmic drops within the electrolyte channel. There are three partially overlapped but differentiable regions in the current-potential curves for different flow rates of CO_2. At the least negative potentials and current densities, ohmic losses and the flux of reactive species are small, meaning the reaction rate is therefore limited by the kinetics which follows the concentration independent Butler-Volmer equation (J_{ac}). At moderate currents, the influence of ohmic drops becomes more apparent and leads to a deviation from the activation-controlled behavior. Although a small concentration

overpotential exists within this potential range represented by the dashed lines, a linear current-potential curve at this potential region is considered to be an indication of rate that is mostly controlled by the electronic and/or ionic resistance.[41] All flow rates exhibited a similar current–potential profile until the CO_2 concentration overpotential becomes more prominent for a specific flow rate. At more negative potentials, the effect of mass transport of CO_2 on the overall potential drop manifests and eventually flattens the current-potential curve as the CO_2 concentrations along the flow channel depletes appreciably. Therefore, conceivably, the effects of flow rates on the

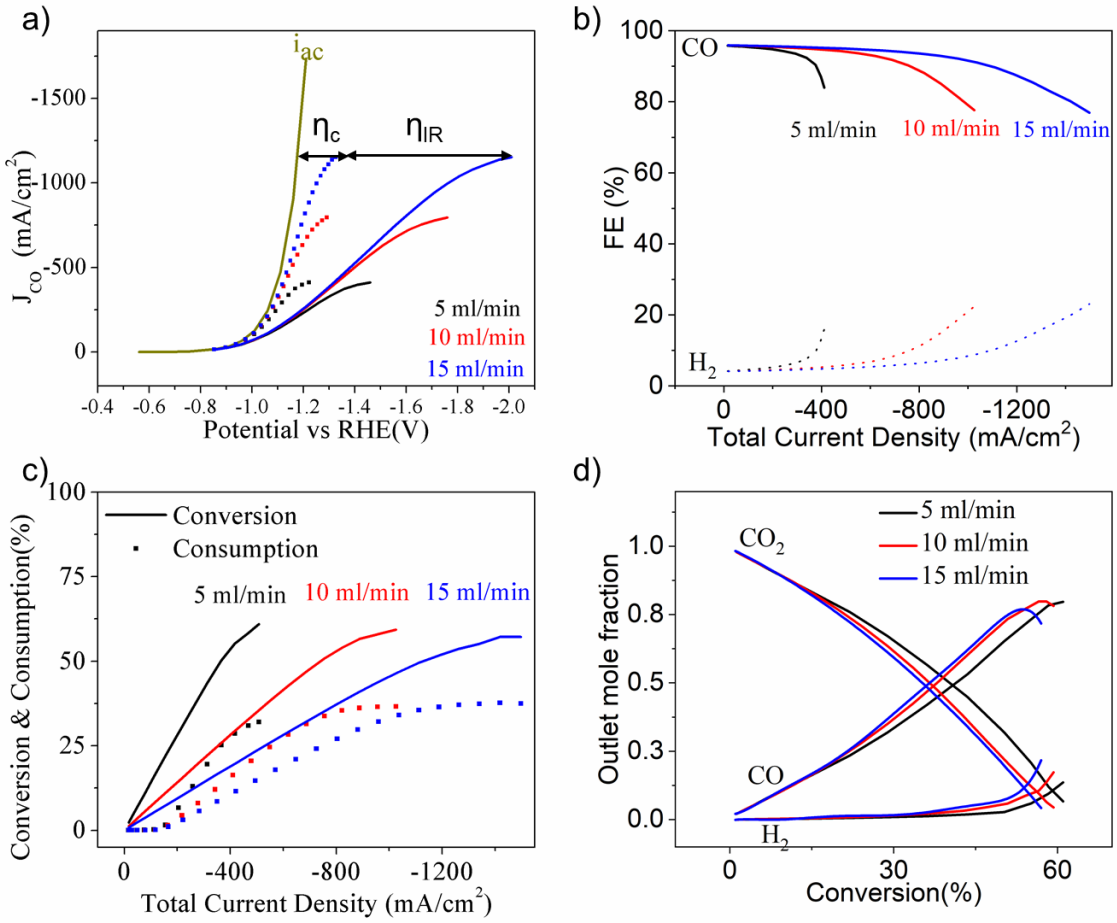

Figure 6: a) Partial current Density of CO vs Potential plots for different flow rate of CO_2 feed gas (solid lines). Dashed Lines and J_{ac} represents the IR corrected and kinetically controlled curves, respectively. **b)** FE of CO and H_2 as a function of total current density for different flow rates. **c)** Electrochemical conversion of CO_2 to CO (solid lines) and homogenous consumption to carbonates (dashed lines) as a function of total current density.**d)** Outlet mole fraction of CO_2, CO and H_2 as function of conversion for different flow rates.

concentration overpotentials and mass transfer limited current density are more apparent at this potential region. However, remarkably, the contribution of ohmic drops to overall potential losses stays considerably high even at the plateau region as the flow rate increases. The contribution of concentration overpotentials to the overall potential loses are around 33% to 18% for 5 and 15 ml min^{-1} flow rates, respectively, at the most extreme computed potential (-1.5 V vs RHE and -2 V vs RHE). Note that we reported results for a relatively high resistance GDL in here to emphasize the effect of ohmic drops which will become more significant as the membrane and electrolyte conductivities are considered. The ohmic loses over GDEs are usually lower when GDLs are compressed with a low contact resistance.

The average faradaic efficiency (FE) in the catalyst layer as a function current density is given in Figure 6b for different flow rates. The depletion of CO_2 along the flow channel results in a selectivity gradient as well (Figure SI8). The relative formation of hydrogen increases with respect to CO as the CO_2 depletes along the channel. Therefore, the overall FE towards CO begins to decline appreciably as the concentration overpotentials becomes significant for each flow rate. Although silver electrodes can provide a high selectivity in a broad range of potentials when excess CO_2 is fed to the electrolyzer, it might be challenging to sustain the same selectivity at high conversions.[42] High flow rates support greater CO_2 flux to the electrode, replenishing the reactants and minimizing the concentration and selectivity gradients along the flow channel, however this happens at the expense of high conversions. In Figure 6c, the single-pass conversion and homogenous consumption of CO_2 are given as a function of total current density for different flow rates. At the same current density, conceivably, lower conversions at high flow rates results in most of the reactant gas to be pushed out the flow channel before it reacts at the electrode surface. When enough potential is applied for each flow rate, the maximum electrochemical conversion of

CO_2 to CO reaches a similar value. This maximum conversion is mostly dictated by the homogenous consumption of CO_2 by the cathodically produced hydroxide which is represented by the dashed lines in Figure 6c. The highest conversion value reaches about 60% for the lowest flow rate, even though the amount of unreacted CO_2 is below 10%. The highest possible conversion exhibits a slight decrease (1-3%) for higher flow rates as a result of a slightly higher alkaline pH at the catalyst layer due to higher reaction rates at high potentials. Although the buffers breakdown eventually at high current densities, the mass transport and buffer capacity of the electrolyte slightly contributes to the consumption rate. For example, an order of magnitude decrease in the electrolyte concentration or the electrolyte flow rate increases the consumption of the CO_2 about 5% and 10%, respectively, which in turn decreases the maximum attainable conversion (Figure SI9). Interestingly, even though the maximum conversion is restricted to below 60%, the outlet fraction of the desired product CO attains a much higher value than the electrochemical conversion because of homogeneous consumption.

The outlet concentrations of CO_2 as a function of conversion are given in Figure 6d for different flow rates, along with the concentrations of CO and H_2. The CO_2 concentrations in the outlet stream exhibit non-linear behavior with a concave downward trend due to homogenous consumption. The increase in the rate of homogenous consumption of CO_2 with increasing flow rates at the same conversion (see Figure 6c) leads to small differences at moderate conversions. At high conversions (>40%), the increase of the rate of HER significantly modifies the outlet concentrations. The mole fraction of CO attains a maximum around 78% until the hydrogen evolution emerges at very high conversions due to concentration overpotentials.[43] All the flow rates exhibit similar trends with small variations (1-4%) in the peak mole fraction. These simulations are in good agreement with a recent experimental study on a MEA type of flow cell

which reported an outlet concentration of around 80 %CO 15% H_2 and 5 % CO_2 at the highest possible conversion.[44] However, the consumption and conversion ratio of CO_2 was different from this study, which is most likely the result of a low electrolyte concentration of bicarbonate used in the anode compartment which indirectly influences the local conditions on the cathode (Figure SI9).

Overall, the results in Figure 6 suggest the increasing flow rate needed to achieve higher current density at the same single-pass conversion and geometric area has conflicting effects. It is desirable to feed a very high amount of CO_2 to achieve high production rates over the same geometrical area, which will significantly decrease the capital costs of a CO_2 electrolyzer. However, modelling suggests the ohmic loses become significant at high flow rates and much higher potentials are required to achieve same single-pass conversion. In addition, the higher applied potentials also cause a decrease in selectivity and lower the outlet concentrations of CO. Therefore, there will a trade-off between current density, applied potential and outlet concentrations at the same conversion. Although increasing the flow rate boosts the production rate, the operational costs due to electricity consumption and separation costs due to more diluted streams might become significant at the same conversion.

The spatial distribution of current density, which is a result of spatial variations of CO_2 partial pressure, electrolyte concentration along the channel and ohmic drops, has both fundamental and practical implications. Although, traditionally, most of the kinetic studies have been conducted using H-cells and rotating disk electrodes in (arguably) well-defined mass transport conditions, there are considerable efforts to carry out kinetic studies and catalyst screening using GDEs,[45, 46] in parallel to what has been done in fuel cell community. [47, 48] Our model suggests that the ohmic drops along the GDE and spatial distributions of reactant and

electrolyte may have an impact on the extracted kinetic parameters such as Tafel slopes, order of the reaction with respect to reactants and overpotentials at a specified current density.[49] The corrections for ohmic drops and mass transfer loses for a GDE are not straightforward and well-established as in the case of rotating disk electrodes. In addition, the selectivity of catalysts will be affected by the concentration gradients along the channel. Although the CO partial pressure at the catalyst layer is not expected to influence the reaction on silver electrodes, for other electrodes, e.g. copper, in which CO is in equilibrium with the electrolyte and surface, changes in the CO partial pressure along channel may impact the selecitivity.[50] The increase in the reaction rates of CO coupling and CO insertion reactions along the channel might alter the selectivity at high conversions. Supplying excess reactant gas and reporting the resistance of the GDE might enable a more accurate comparison of the specific activities of the electrocatalysts for fundamental studies. Regardless of the how high the tested current density or geometrical surface area are, an excess amount of CO_2 will ensure a minimal concentration gradient along the channel. In fact, a majority of reported studies in literature have used excess reactant gas supply while there has been a recent push to study effect on single-pass conversion on the performance of the flow cells.).[13, 16, 46, 51, 52] Sargent and co-workers reported record partial current density of CO_2 reduction to ethylene above 1 A cm^{-2} on a 1 cm^2 electrode, but the single pass conversions are typically low (<10%) because of the supply of high flow rates.[16] In contrast, Kanan and co-workers achieved high single-pass CO conversions (>50%) on copper electrodes at a moderate current density range (100-200 mA cm^{-2}) with electrode geometrical area around 1 cm^2 by using a very small flow rates (<1ml/min).[53] Therefore, the single-pass conversion may serve as a qualitative indication for the extent of concentration gradients along the GDE and flow channel rather than the current density.

Unlike fundamental studies, practical applications require high single-pass conversion to minimize the energy-intensive downstream separation which will most likely affect both capital and operational costs.[54] Implementation of CO_2 electrolysis at a large scale will highly benefit from low cell voltages and high single-pass coversions.[55, 56] At high conversions, however, the outlet concentration of CO_2 will eventually be low. Therefore, a concentration gradient from inlet to outlet is inevitable. To achieve maximum conversion with minimal concentration overpotential and selectivity loses, a catalyst that is active and selective in a broad range of potentials is desirable. Modelling studies to optimize flow patterns and engineering studies to introduce turbulent mixing in the flow channel may also help to minimize these losses along the flow channel at high single pass conversions. In addition, the concentration gradients not only impact the energy efficiency and selectivity but also might influence the stability of the GDE and the system. Uneven current density gradients along the GDL may cause accelerated electrode degradation and flooding where the local current density is higher.

The results presented from this model depend on the dimensions of the flow cell and material parameters of the GDE. The effect of the geometric area and flow patterns to single pass conversion and outlet concentrations are a particularly unexplored yet vital area of research. In addition, the materials used in CO_2 electrolysis are mostly transferred from fuel cell research. Although the effect of materials parameters to the selectivity and activity is not considered to be as significant as process parameters and cell dimentsions,[57] preparation of custom GDLs for CO_2 electrolysis might be beneficial especially to mitigate flooding issues and improve water management.[29] Furthermore, although Nafion ionomer and/or PTFE binders can supply hydrophobic regions for gas supply,[58, 59] the CL can be partially saturated with electrolyte depending the distribution of the hydrophobic regions at the surface and interaction with liquid

water. The liquid saturation degree of the CL will influence the diffusion layer thickness and diffusivity of the reactants and products.[27] Consequently, CO_2 concentration gradients across the catalyst layer might develop depending on the saturation level which will impact the selectivity of the process and therefore the outlet concentrations. Moreover, the protons produced at the anode may cause bubbling out of CO_2 at high current densities either at the anode or cathode compartment depending on the type of ion exchange membrane used.[14, 17] This may cause a change in the bulk pH and may indirectly effect the local conditions of the catholyte and/or anolyte if the total volume and/or flow rate of the electrolyte are low. Last but not least, the local conditions in the anode and the ion flux through the membrane might directly influence the local conditions along the catholyte chamber if the thickness of the electrolyte channel is smaller than the boundary layer thickness.

Conclusions

The 2-D modelling study presented here quantifies the concentration gradients along a flow cell during CO_2 electroreduction, and discusses their fundamental and practical implications. The concentration of buffer anions diminishes along the electrolyte flow channel, which results in a variant boundary layer thickness (1-200 μm) and gradient of local pH (3 pH units) along the CL. The concentration of CO_2 also depletes along the flow channel as a result of electrochemical conversion at the electrode and non-electrochemical consumption by the electrolyte. Together with the ohmic drops, this leads to a spatially variant current density along and across the CL. The effect of CO_2 concentration overpotential losses over ohmic drops becomes significant at very high conversions, however, the contribution of concentration overpotential to overall potential loses decreases with increasing flow rates of CO_2 feed gas. Although the maximum conversion is limited to below 60% (depending on the buffer capacity and flow rate of the electrolyte), the outlet concentration of CO attains a maximum to about 75-80% along with 5-10 % CO_2 and 10-15% H_2

at high conversions depending on the flow rate. Even though the quantitative nature of this model is not directly applicable since the experimental studies are highly variant in terms of space, time and length, we hope the model will provide guidelines to fundamental studies and insights to practical studies targeting high single pass conversions.

Acknowledgments

This work was authored in part by the National Renewable Energy Laboratory (NREL), operated by Alliance for Sustainable Energy, LLC, for the U.S. Department of Energy (DOE) under Contract No. DE-AC36-08GO28308. This work was supported by the Laboratory Directed Research and Development (LDRD) Program at NREL. The views expressed in the article do not necessarily represent the views of the DOE or the U.S. Government. The U.S. Government retains and the publisher, by accepting the article for publication, acknowledges that the U.S. Government retains a nonexclusive, paid-up, irrevocable, worldwide license to publish or reproduce the published form of this work, or allow others to do so, for U.S. Government purposes.

References

1. Kibria, M. G.; Edwards, J. P.; Gabardo, C. M.; Dinh, C. T.; Seifitokaldani, A.; Sinton, D.; Sargent, E. H., Electrochemical CO2 reduction into chemical feedstocks: from mechanistic electrocatalysis models to system design. *Advanced Materials* **2019,** *31* (31), 1807166.
2. Kondratenko, E. V.; Mul, G.; Baltrusaitis, J.; Larrazábal, G. O.; Pérez-Ramírez, J., Status and perspectives of CO 2 conversion into fuels and chemicals by catalytic, photocatalytic and electrocatalytic processes. *Energy & environmental science* **2013,** *6* (11), 3112-3135.
3. Birdja, Y. Y.; Pérez-Gallent, E.; Figueiredo, M. C.; Göttle, A. J.; Calle-Vallejo, F.; Koper, M. T., Advances and challenges in understanding the electrocatalytic conversion of carbon dioxide to fuels. *Nature Energy* **2019,** *4* (9), 732-745.
4. Burdyny, T.; Smith, W. A., CO 2 reduction on gas-diffusion electrodes and why catalytic performance must be assessed at commercially-relevant conditions. *Energy & Environmental Science* **2019,** *12* (5), 1442-1453.
5. Higgins, D.; Hahn, C.; Xiang, C.; Jaramillo, T. F.; Weber, A. Z., Gas-diffusion electrodes for carbon dioxide reduction: A new paradigm. *ACS Energy Letters* **2018,** *4* (1), 317-324.

6. Philips, M. F.; Gruter, G.-J. M.; Koper, M. T.; Schouten, K. J. P., Optimizing the Electrochemical Reduction of CO2 to Formate: A State-of-the-Art Analysis. *ACS Sustainable Chemistry & Engineering* **2020**.
7. Sedighian Rasouli, A.; Wang, X.; Wicks, J.; Lee, G.; Peng, T.; Li, F.; McCallum, C.; Dinh, C.-T.; Ip, A. H.; Sinton, D., CO2 electroreduction to methane at production rates exceeding 100 mA/cm2. *ACS Sustainable Chemistry & Engineering* **2020**.
8. Endrődi, B.; Kecsenovity, E.; Samu, A.; Darvas, F.; Jones, R.; Török, V.; Danyi, A.; Janáky, C., Multilayer electrolyzer stack converts carbon dioxide to gas products at high pressure with high efficiency. *ACS energy letters* **2019,** *4* (7), 1770-1777.
9. Vennekoetter, J.-B.; Sengpiel, R.; Wessling, M., Beyond the catalyst: How electrode and reactor design determine the product spectrum during electrochemical CO2 reduction. *Chemical Engineering Journal* **2019,** *364*, 89-101.
10. Kas, R.; Yang, K.; Bohra, D.; Kortlever, R.; Burdyny, T.; Smith, W. A., Electrochemical CO 2 reduction on nanostructured metal electrodes: fact or defect? *Chemical Science* **2020,** *11* (7), 1738-1749.
11. Weekes, D. M.; Salvatore, D. A.; Reyes, A.; Huang, A.; Berlinguette, C. P., Electrolytic CO2 reduction in a flow cell. *Accounts of chemical research* **2018,** *51* (4), 910-918.
12. Verma, S.; Lu, X.; Ma, S.; Masel, R. I.; Kenis, P. J., The effect of electrolyte composition on the electroreduction of CO 2 to CO on Ag based gas diffusion electrodes. *Physical Chemistry Chemical Physics* **2016,** *18* (10), 7075-7084.
13. Ma, S.; Sadakiyo, M.; Luo, R.; Heima, M.; Yamauchi, M.; Kenis, P. J., One-step electrosynthesis of ethylene and ethanol from CO2 in an alkaline electrolyzer. *Journal of Power Sources* **2016,** *301*, 219-228.
14. Endrődi, B.; Bencsik, G.; Darvas, F.; Jones, R.; Rajeshwar, K.; Janáky, C., Continuous-flow electroreduction of carbon dioxide. *Progress in Energy and Combustion Science* **2017,** *62*, 133-154.
15. Hernandez-Aldave, S.; Andreoli, E., Fundamentals of Gas Diffusion Electrodes and Electrolysers for Carbon Dioxide Utilisation: Challenges and Opportunities. *Catalysts* **2020,** *10* (6), 713.
16. De Arquer, F. P. G.; Dinh, C.-T.; Ozden, A.; Wicks, J.; McCallum, C.; Kirmani, A. R.; Nam, D.-H.; Gabardo, C.; Seifitokaldani, A.; Wang, X., CO2 electrolysis to multicarbon products at activities greater than 1 A cm− 2. *Science* **2020,** *367* (6478), 661-666.
17. Ma, M.; Clark, E. L.; Therkildsen, K. T.; Dalsgaard, S.; Chorkendorff, I.; Seger, B., Insights into the carbon balance for CO 2 electroreduction on Cu using gas diffusion electrode reactor designs. *Energy & Environmental Science* **2020,** *13* (3), 977-985.
18. Chen, Y.; Vise, A.; Klein, W. E.; Cetinbas, F. C.; Kariuki, N. N.; Myers, D. J.; Smith, W. A.; Deutsch, T. G.; Neyerlin, K. C., A robust, scalable platform for the electrochemical conversion of CO2 to formate; identifying pathways to higher energy efficiencies. *ACS Energy Letters* **2020**.
19. Lee, W.; Kim, Y. E.; Youn, M. H.; Jeong, S. K.; Park, K. T., Catholyte-free electrocatalytic CO2 reduction to formate. *Angewandte Chemie International Edition* **2018,** *57* (23), 6883-6887.
20. Yang, H.; Kaczur, J. J.; Sajjad, S. D.; Masel, R. I., CO2 conversion to formic acid in a three compartment cell with Sustainion™ membranes. *ECS Transactions* **2017,** *77* (11), 1425.
21. Xia, C.; Zhu, P.; Jiang, Q.; Pan, Y.; Liang, W.; Stavitsk, E.; Alshareef, H. N.; Wang, H., Continuous production of pure liquid fuel solutions via electrocatalytic CO 2 reduction using solid-electrolyte devices. *Nature Energy* **2019,** *4* (9), 776-785.
22. Dinh, C.-T.; Burdyny, T.; Kibria, M. G.; Seifitokaldani, A.; Gabardo, C. M.; De Arquer, F. P. G.; Kiani, A.; Edwards, J. P.; De Luna, P.; Bushuyev, O. S., CO2 electroreduction to ethylene via hydroxide-mediated copper catalysis at an abrupt interface. *Science* **2018,** *360* (6390), 783-787.
23. Brée, L. C.; Wessling, M.; Mitsos, A., Modular modeling of Electrochemical Reactors: Comparison of CO2-Electolyzers. *Computers & Chemical Engineering* **2020**, 106890.
24. Chen, Y.; Xiang, C.; Lewis, N., Modeling the Performance of A Flow-Through Gas Diffusion Electrode for Electrochemical Reduction of CO or CO 2. *Journal of the Electrochemical Society* **2020**.

25. Wu, K.; Birgersson, E.; Kim, B.; Kenis, P. J.; Karimi, I. A., Modeling and experimental validation of electrochemical reduction of CO2 to CO in a microfluidic cell. *Journal of The Electrochemical Society* **2014,** *162* (1), F23.
26. Weng, L.-C.; Bell, A. T.; Weber, A. Z., Towards membrane-electrode assembly systems for CO 2 reduction: a modeling study. *Energy & Environmental Science* **2019,** *12* (6), 1950-1968.
27. Weng, L.-C.; Bell, A. T.; Weber, A. Z., Modeling gas-diffusion electrodes for CO 2 reduction. *Physical Chemistry Chemical Physics* **2018,** *20* (25), 16973-16984.
28. El-Kharouf, A.; Mason, T. J.; Brett, D. J.; Pollet, B. G., Ex-situ characterisation of gas diffusion layers for proton exchange membrane fuel cells. *Journal of Power Sources* **2012,** *218*, 393-404.
29. Reyes, A.; Jansonius, R. P.; Mowbray, B. A.; Cao, Y.; Wheeler, D. G.; Chau, J.; Dvorak, D. J.; Berlinguette, C. P., Managing hydration at the cathode enables efficient CO2 electrolysis at commercially relevant current densities. *ACS Energy Letters* **2020,** *5* (5), 1612-1618.
30. Zhao, J.; Shahgaldi, S.; Ozden, A.; Alaefour, I. E.; Li, X.; Hamdullahpur, F., Effect of catalyst deposition on electrode structure, mass transport and performance of polymer electrolyte membrane fuel cells. *Applied Energy* **2019,** *255*, 113802.
31. Ren, X.; Myles, T. D.; Grew, K. N.; Chiu, W. K., Carbon dioxide transport in Nafion 1100 EW membrane and in a direct methanol fuel cell. *Journal of The Electrochemical Society* **2015,** *162* (10), F1221.
32. Sethuraman, V. A.; Khan, S.; Jur, J. S.; Haug, A. T.; Weidner, J. W., Measuring oxygen, carbon monoxide and hydrogen sulfide diffusion coefficient and solubility in Nafion membranes. *Electrochimica Acta* **2009,** *54* (27), 6850-6860.
33. Jee, M. S.; Jeon, H. S.; Kim, C.; Lee, H.; Koh, J. H.; Cho, J.; Min, B. K.; Hwang, Y. J., Enhancement in carbon dioxide activity and stability on nanostructured silver electrode and the role of oxygen. *Applied Catalysis B: Environmental* **2016,** *180*, 372-378.
34. Kostecki, R.; Augustynski, J., Electrochemical reduction of CO2 at an activated silver electrode. *Berichte der Bunsengesellschaft für physikalische Chemie* **1994,** *98* (12), 1510-1515.
35. Kita, H., Periodic variation of exchange current density of hydrogen electrode reaction with atomic number and reaction mechanism. *Journal of the Electrochemical Society* **1966,** *113* (11), 1095.
36. Kas, R.; Kortlever, R.; Yılmaz, H.; Koper, M. T.; Mul, G., Manipulating the hydrocarbon selectivity of copper nanoparticles in CO2 electroreduction by process conditions. *ChemElectroChem* **2015,** *2* (3), 354-358.
37. Resasco, J.; Lum, Y.; Clark, E.; Zeledon, J. Z.; Bell, A. T., Effects of anion identity and concentration on electrochemical reduction of CO2. *ChemElectroChem* **2018,** *5* (7), 1064-1072.
38. Yang, K.; Kas, R.; Smith, W. A., In situ infrared spectroscopy reveals persistent alkalinity near electrode surfaces during CO2 electroreduction. *Journal of the American Chemical Society* **2019,** *141* (40), 15891-15900.
39. Burdyny, T.; Graham, P. J.; Pang, Y.; Dinh, C.-T.; Liu, M.; Sargent, E. H.; Sinton, D., Nanomorphology-enhanced gas-evolution intensifies CO2 reduction electrochemistry. *ACS Sustainable Chemistry & Engineering* **2017,** *5* (5), 4031-4040.
40. Zhang, Z.; Melo, L.; Jansonius, R. P.; Habibzadeh, F.; Grant, E. R.; Berlinguette, C. P., pH Matters When Reducing CO2 in an Electrochemical Flow Cell. *ACS Energy Letters* **2020,** *5*, 3101-3107.
41. Yu, D.; Yuvarajan, S., Electronic circuit model for proton exchange membrane fuel cells. *Journal of Power Sources* **2005,** *142* (1-2), 238-242.
42. Jeanty, P.; Scherer, C.; Magori, E.; Wiesner-Fleischer, K.; Hinrichsen, O.; Fleischer, M., Upscaling and continuous operation of electrochemical CO2 to CO conversion in aqueous solutions on silver gas diffusion electrodes. *Journal of CO2 Utilization* **2018,** *24*, 454-462.
43. Kim, B.; Ma, S.; Jhong, H.-R. M.; Kenis, P. J., Influence of dilute feed and pH on electrochemical reduction of CO2 to CO on Ag in a continuous flow electrolyzer. *Electrochimica Acta* **2015,** *166*, 271-276.

44. Jeng, E.; Jiao, F., Investigation of CO 2 Single-Pass Conversion in a Flow Electrolyzer. *Reaction Chemistry & Engineering* **2020**.
45. Inaba, M.; Jensen, A. W.; Sievers, G. W.; Escudero-Escribano, M.; Zana, A.; Arenz, M., Benchmarking high surface area electrocatalysts in a gas diffusion electrode: measurement of oxygen reduction activities under realistic conditions. *Energy & environmental science* **2018,** *11* (4), 988-994.
46. De Gregorio, G. L.; Burdyny, T.; Loiudice, A.; Iyengar, P.; Smith, W. A.; Buonsanti, R., Facet-dependent selectivity of Cu catalysts in electrochemical CO2 reduction at commercially viable current densities. *ACS catalysis* **2020,** *10* (9), 4854-4862.
47. Neyerlin, K.; Gu, W.; Jorne, J.; Gasteiger, H. A., Study of the exchange current density for the hydrogen oxidation and evolution reactions. *Journal of The Electrochemical Society* **2007,** *154* (7), B631.
48. Neyerlin, K.; Gu, W.; Jorne, J.; Gasteiger, H. A., Determination of catalyst unique parameters for the oxygen reduction reaction in a PEMFC. *Journal of the Electrochemical Society* **2006,** *153* (10), A1955.
49. Kubannek, F.; Turek, T.; Krewer, U., Modeling oxygen gas diffusion electrodes for various technical applications. *Chemie Ingenieur Technik* **2019,** *91* (6), 720-733.
50. Wuttig, A.; Liu, C.; Peng, Q.; Yaguchi, M.; Hendon, C. H.; Motobayashi, K.; Ye, S.; Osawa, M.; Surendranath, Y., Tracking a common surface-bound intermediate during CO2-to-fuels catalysis. *ACS central science* **2016,** *2* (8), 522-528.
51. Lv, J. J.; Jouny, M.; Luc, W.; Zhu, W.; Zhu, J. J.; Jiao, F., A highly porous copper electrocatalyst for carbon dioxide reduction. *Advanced Materials* **2018,** *30* (49), 1803111.
52. Wang, R.; Haspel, H.; Pustovarenko, A.; Dikhtiarenko, A.; Russkikh, A.; Shterk, G.; Osadchii, D.; Ould-Chikh, S.; Ma, M.; Smith, W. A., Maximizing Ag utilization in high-rate CO2 electrochemical reduction with a coordination polymer-mediated gas diffusion electrode. *ACS Energy Letters* **2019,** *4* (8), 2024-2031.
53. Ripatti, D. S.; Veltman, T. R.; Kanan, M. W., Carbon monoxide gas diffusion electrolysis that produces concentrated C2 products with high single-pass conversion. *Joule* **2019,** *3* (1), 240-256.
54. Jouny, M.; Luc, W.; Jiao, F., General techno-economic analysis of CO2 electrolysis systems. *Industrial & Engineering Chemistry Research* **2018,** *57* (6), 2165-2177.
55. Verma, S.; Kim, B.; Jhong, H. R. M.; Ma, S.; Kenis, P. J., A gross-margin model for defining technoeconomic benchmarks in the electroreduction of CO2. *ChemSusChem* **2016,** *9* (15), 1972-1979.
56. Salvatore, D.; Berlinguette, C. P., Voltage Matters When Reducing CO2 in an Electrochemical Flow Cell. *ACS Energy Letters* **2019,** *5* (1), 215-220.
57. Liang, S.; Altaf, N.; Huang, L.; Gao, Y.; Wang, Q., Electrolytic cell design for electrochemical CO2 reduction. *Journal of CO2 Utilization* **2020,** *35*, 90-105.
58. Wilson, M. S.; Gottesfeld, S., Thin-film catalyst layers for polymer electrolyte fuel cell electrodes. *Journal of applied electrochemistry* **1992,** *22* (1), 1-7.
59. Perry, M. L.; Newman, J.; Cairns, E. J., Mass transport in gas-diffusion electrodes: a diagnostic tool for fuel-cell cathodes. *Journal of the Electrochemical Society* **1998,** *145* (1), 5.